A strangely light neutron star

Victor Doroshenko (doroshv@astro.uni-tuebingen.de)
Institut fuer Astronomie und Astrophysik, Universitaet Tuebingen https://orcid.org/0000-0001-8162-1105

Valery Suleimanov
University of Tübingen https://orcid.org/0000-0003-3733-7267

Gerd Pühlhofer
https://orcid.org/0000-0003-4632-4644

Andrea Santangelo
Institut fuer Astronomie und Astrophysik, Universitaet Tuebingen

Article

Keywords:

Posted Date: April 5th, 2022

DOI: https://doi.org/10.21203/rs.3.rs-1509469/v1

Version of Record: A version of this preprint was published at Nature Astronomy on October 24th, 2022.
See the published version at https://doi.org/10.1038/s41550-022-01800-1.

A strangely light neutron star

Victor Doroshenko[1*], Valery Suleimanov[1], Gerd Pühlhofer[1] and Andrea Santangelo[1]

[1*]Institut für Astronomie und Astrophysik, Sand 1, Tuebingen, 72076, Germany.

*Corresponding author(s). E-mail(s): doroshv@astro.uni-tuebingen.de;

To constrain the equation of state of cold dense matter, astrophysical measurements are essential. These are mostly based on observations of neutron stars in the X-ray band, and, more recently, also on gravitational wave observations. Of particular interest are observations of unusually heavy or light neutron stars which extend the range of central densities probed by observations and thus permit testing nuclear physics predictions over a wider parameter space. Here we report on the analysis of such a star, a central compact object within the supernova remnant HESS J1731-347. We estimate the mass and radius of the neutron star to be $M = 0.77^{+0.20}_{-0.17}\,M_{\odot}$ and $R = 10.4^{+0.86}_{-0.78}$ km, respectively, based on modeling of the X-ray spectrum and a robust distance estimate from Gaia observations. Our estimate implies that this object is either the lightest neutron star known, or a "strange star" with a more exotic equation of state. Adopting a standard neutron star matter hypothesis significantly constrains the corresponding equations of state.

Central compact objects (CCOs) are isolated, radio quiet, non-accreting, thermally emitting neutron stars found at the centres of Supernova Remnants (SNRs) [1–3]. Their thermal X-ray emission is believed to be associated with the cooling of young, weakly magnetised [4, 5] neutron stars and comes from the atmosphere covering a large fraction of the surface. Most CCOs exhibit no pulsations, which suggests a rather uniform temperature distribution over the NS surface. This implies that the uncertainties associated with the geometry of the emission region, the details of the accretion physics, and the radiative

transfer in strong magnetic fields which are all typical of accreting NS are irrelevant for CCOs. Such simplicity makes CCOs ideal laboratories to investigate the equation of state of dense matter [6, 7].

On the other hand, CCOs are only observed as faint X-ray sources, and often lack reliable distance and luminosity estimates, which translates to large uncertainties in the emission area and neutron star radius estimates [8–10]. Furthermore, the lack of detected pulsations does not necessarily imply that the entire surface emits uniformly, and could be simply due to an unfavourable orientation of the observer's line of sight with respect to the spin and magnetic dipole axes of the NS [11, 12]. The composition of the atmosphere also significantly influences the estimated neutron star parameters. In particular, atmospheres composed of carbon, or even heavier elements, have been suggested for a significant fraction of CCOs [13–15].

We emphasize, however, that the caveats outlined above are now largely sorted out. With regard to atmosphere composition, hydrogen atmospheres yield unreasonably small neutron star radii [9, 10], whereas emission from atmospheres with even heavier compositions strongly deviate from the observed black-body like spectra [13]. Instead of deducing unreasonably small neutron star radii, one could assume that the emission originates from a fraction of the neutron star surface and pulsations are not observed only because of an unfavorable viewing orientation. This is, however, in conflict with the existing limits on the amplitude of potential pulsations ($\sim 8\%$ for the CCO in HESS 1731-347 [12] and less than $\sim 12\%$ for the CCO in Cas A [16, 17] and in range 3-50% for other objects). Note that although probabilities quoted above for individual objects are not negligible, missing pulsations from all non-pulsating CCOs is highly unlikely with a chance probability estimated to be $\leq 10^{-6}$ [16].

Considering that there are currently no other ideas to explain the observed thermal non-pulsed emission, uniformly emitting carbon atmospheres appear to be the only viable option to explain the observed spectra of CCOs. The largest remaining source of uncertainty to estimate neutron star parameters comes from the poorly constrained distances to most CCOs. There are, however, a couple of fortunate exceptions, most notably the CCO in SNR HESS J1731-347 which is the subject of the investigation presented in this paper.

Results

The CCO in SNR HESS J1731−347 happens to be the brightest and one of the most observed objects of its kind. Recently, we were able to unambiguously show that besides the CCO, there is also an optical star in the centre of the remnant [18]. This conclusion is mostly based on the fact that the estimated mass of a thick dust shell, in which the optical star and the compact object are embedded, is $\sim 2M_{\odot}$, and by far exceeds what could be produced by the star itself. The dust shell can, therefore, only originate from supernova ejecta, so both the shell and the optical star definitively reside within the SNR (irrespective of their evolutionary relation or lack thereof) and at the same

distance to Earth. The distance to the optical companion is well constrained by Gaia parallax measurements to 2.5(3) kpc [19].

This estimate is independently confirmed by the analysis of the spatial profile of the dust scattering halo observed around the CCO [20] when considering the 3-D distribution of dust along the line of sight, which was independently derived by [21]. The only other CCO to which the distance is known with comparable accuracy is the one in Cas A. This CCO is, however, not only a factor of two fainter, but is also submerged within a compact bright SNR, which significantly contributes to the observed background for instruments with moderate angular resolution such as XMM-*Newton* which provide the large effective areas needed for the presented work. The case of HESS J1731−347 presents, therefore, a unique opportunity to study a CCO with a reliably constrained distance and high counting statistics provided by extensive XMM-*Newton* observations, and permits to derive meaningful constraints on the mass and radius of a thermally emitting isolated neutron star.

To achieve this goal, we re-analyzed all available X-ray observations of the source (taken in imaging modes, see Methods for detail), and modeled the observed X-ray spectrum using state-of the art atmosphere models using the Gaia distance as a prior for model normalisation. We also took into account the contamination of the observed point source spectrum by the compact dust halo, which partially falls within the point spread function of the X-ray telescopes used to observe the source. As a result, we find that the observed spectral shape and absence of detectable pulsations can only be reconciled with each other if the emission comes from an atmosphere of a neutron star composed predominantly of carbon and with an essentially uniform temperature distribution (see Methods for details). Under this assumption and taking the Gaia parallax measurement into account, we estimate $M = 0.77^{+0.20}_{-0.17} M_{\odot}$ and $R = 10.4^{+0.86}_{-0.78}$ km for the neutron star (uncertainties are reported at 1σ confidence level throughout the text unless stated otherwise).

Discussion

Our mass estimate makes the CCO in HESS J1731-347 the lightest neutron star known to date, and potentially a more exotic object, i.e. a "strange star" candidate. We emphasize that while the first part of the statement above is a robust result, the second is an intriguing possibility which is consistent with our analysis. However, the obtained constraints on mass and radius are still fully consistent with a standard neutron star interpretation and can be used to improve astrophysical constraints on the equation of state of cold dense matter under this assumption. The latter point can be illustrated by taking into account the available prior information for the EOS of cold dense matter when modeling the X-ray spectrum of the CCO. In particular, we use the family of EOSs published by [22, 23] to define the priors for mass and radius of the neutron star. The papers mentioned above combine nuclear-theory calculations of the EOS with tidal deformability constraints deduced from the gravitational wave

events GW190425 and GW170817 (including their electromagnetic counterparts AT2017gfo and GRB170817A, respectively), radio-based mass measurements for PSR J0740+6620, PSR J0348+4042, and PSR J1614-2230, and NICER measurements of the mass and radius of PSR J0030+0451 and PSR J0740+6620 based on the analysis of X-ray pulse profiles. In addition to that, we also included constraints by [24] based on modelling of the burst spectra of the X-ray burster 4U 1702-429 and from the rotation limit for the radio pulsar PSR J1748−2446ad [25]. Finally, full Gaia distance priors for the CCO as derived for the companion star by [19] were incorporated.

The results are presented in Fig. 1, which illustrates that while our measurement is consistent with the aforementioned results, the range of allowed theoretical models is substantially reduced when our result is taken into consideration. Taking the extra priors into account also allows us to further improve constraints on the mass and radius of the CCO, resulting in $M = 0.83^{+0.17}_{-0.13} M_{\odot}$ and $R = 11.25^{+0.53}_{-0.37}$ km, respectively. The corresponding radius of a "standard" $1.4 M_{\odot}$ neutron star allowed by all EOSs that are consistent with this estimate is $R_{1.4} = 11.68^{+0.52}_{-0.50}$ km (at 90% confidence level). This estimate is a useful metric for comparing the effect that various astrophysical constraints have on the EOS. One can compare our value with that reported by [23] who find $R_{1.4} = 11.94^{+0.76}_{-0.87}$ km at the same confidence level.

We emphasize that the inclusion of the extra prior information mostly affects the estimate of the radius of the neutron star, whereas the derived mass remains unprecedentedly low. Such a light neutron star, regardless of the assumed internal composition, appears to be a very intriguing object from an astrophysical perspective. Indeed, forming NSs with masses lower than $\sim 1.17 M_{\odot}$ is problematic [28] from an evolutionary perspective, and the least massive neutron star known to date (PSR J0453+1559 with an estimated mass of $1.174 \pm 0.004 M_{\odot}$) has been compatible with this constraint. Our estimate for the mass of the CCO in HESS J1731-347 is only marginally consistent with this limit, which might be important for testing theoretical estimates for the minimal neutron star mass, and for understanding the origin of CCOs.

Methods

Parallax and distance priors

A key difference of this work with respect to past analyses of the source by [10, 14] is that the distance to the source is not assumed, but can rather be considered as a free parameter with priors defined by the Gaia EDR3 parallax measurement. The optical counterpart of the CCO was identified by [18] and corresponds to Gaia EDR3 source 5975119332093959552, for which a parallax of 0.38(4) mas has been measured. As discussed by [19], a simple inversion of Gaia parallaxes can result in biased distance estimates because inversion implies that the uncertainty on distance is no more normally distributed (for instance, distance can not be negative), and is affected by which stars can actually be observed with Gaia in a given direction, taking into account the instrument sensitivity

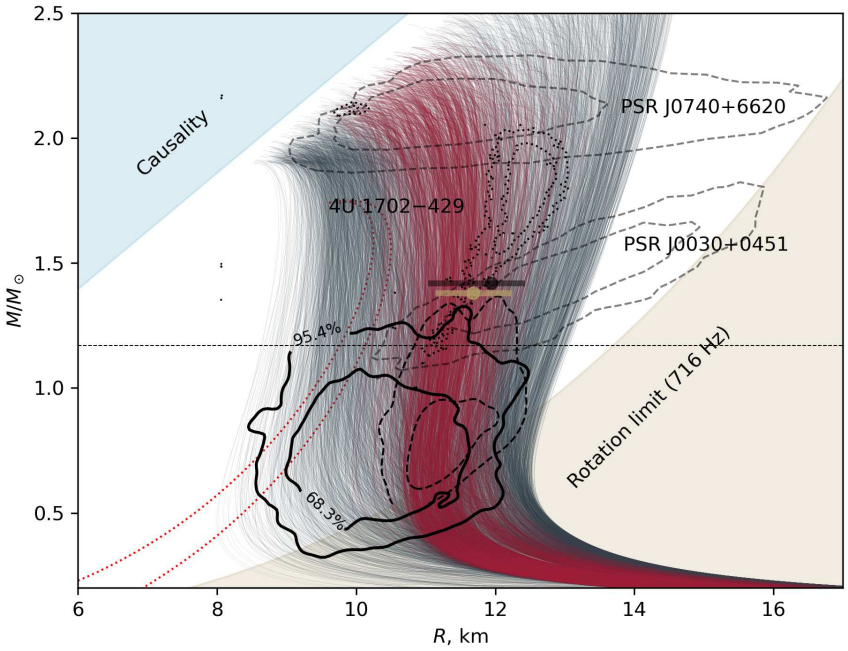

Fig. 1 Equation of state predictions and observational constraints, as a function of the radius and mass of the compact star. The contours show mass and radius constraints for PSR J0740+6620 and PSR J0030+0451 reported by [26, 27] based on the NICER data, and for CCO in HESS J1731-347 obtained in this work. Here, the thick solid line corresponds to the case when only parallax priors and X-ray data are considered, whereas the thick dashed lines correspond to the joint fit including all prior information as discussed in the text. All contours are plotted for the same 68.3 and 95.4% confidence levels. The collection of thin black lines represents the family of chiral EOSs considered by [22, 23], with red lines on top indicating the EOSs that are allowed by the combined analysis of priors by [26, 27], constrains based on the analysis of X-ray bursts from 4U 1702-429 by [24], and this work (90% confidence). Two representative strange quark matter (SQM) EOSs are also plotted for completeness (red dashed lines). The error bars around $1.4M_\odot$ show the expected radius of a "standard" neutron star allowed by EOS constraints by [27] (black), and in this work (beige, both at 90% confidence level). The horizontal dashed line shows a lower limit on the expected astrophysical NS mass by [28].

and extinction (i.e. zero parallax does not necessarily imply infinite distance). However, these caveats are mostly relevant for objects with poorly constrained parallaxes, which does not apply to the source. Therefore, we start our modelling by simply using a parallax to define priors for normalization of the atmosphere models. We note that the model normalization is inversely proportional to distance and parallax squared, so the inversion problem mentioned above is not relevant here. We also correct for known zero point offsets in parallaxes measured with Gaia, where the correction is calculated after [29] using the code made available by the Gaia collaboration[1] to be -27,239 micro-as. As a cross-check, we also used the full geometric distance prior given by Eq 3 in

[1] https://www.cosmos.esa.int/web/gaia/edr3-code

[19] with parameters α, β, L taken from the associated catalog[2] for the case when all other priors on the NS EOS are included; however, the difference with respect to simple parallax inversion was found to be negligible in our case. Finally, we note that in both cases (i.e. both for simple parallax inversion and more sophisticated distance priors) there is also some uncertainty in the true value of the adopted parallax zero point value. Indeed, besides estimates by the Gaia collaboration (i.e. [29] used here), there are multiple attempts to estimate it by contrasting the Gaia parallax measurements with independent distance estimates obtained for various object types [30–32]. Deviations are, however, on average consistent with zero, and in no case were found to be larger than ~ 0.02 mas. We can safely conclude, therefore, that in our case the distance estimate is dominated by the statistical uncertainty of the parallax. Moreover, most of the works cited above find offsets either consistent or slightly smaller than found by [29], i.e. that the latter work might underestimate the true parallaxes slightly. In the context of our work, this would imply a smaller distance and even smaller mass/radius of the neutron star.

Finally, it is worth noting that, besides geometric priors, [19] also provide distance estimates based on photo-geometric priors, which could be more accurate for sources with poorly constrained parallaxes, and gives an even lower distance (~ 2.2 vs ~ 2.5 kpc). We note, however, that the presence of the dust shell around the optical star, and complex absorption in the direction of the source might bias distance photo-geometric estimate with respect to the purely geometric priors which are rather well defined in our case. Again, in the context of our work, a lower distance would imply an even lower neutron star mass, so geometric priors appear to be a safer and more conservative choice.

X-ray data reduction

For spectral analysis, we used all data obtained with the XMM-*Newton* observatory in imaging modes (i.e. the same data as in [14]). In addition to that, we also used a single 40 ks long *Suzaku* observation of the source (obsid. 401099010). All observations were reduced using current versions of XMM SAS (`xmmsas_20210316_1931`), *HEASOFT* (6.29c) and current calibration files (XMM-CCF-REL-386 for XMM-*Newton*, CalDB 4.9.4 for *Chandra*, and 20181010 for *Suzaku*). For XMM-*Newton* observations, the source spectra were extracted from a source-centred region with a radius of 50″ (optimised for best signal-to-noise ratio using the *eregionanalyse* task). The background was extracted from nearby source-free regions around the source as recommended in the XMM-*Newton* documentation (that is, source-centred annuli with radius 90-200″ for the MOS cameras and a 90″ circle to the side of the source with the same raw Y coordinate as the source for the PN camera). For *Suzaku*, source spectra were extracted from a source-centred circular region with radius of 200″ and background from an annulus with an inner radius of 260″ and an outer radius of 400″. We have verified that the spectral analysis results are not significantly affected by a different choice of the background regions, which

[2] https://www2.mpia-hd.mpg.de/homes/calj/gedr3_distances/main.html

is expected given the comparatively low surface brightness of the extended emission from the SNR (which dominates the astrophysical background), and is consistent with earlier findings by [14]. The extracted spectra were binned to contain at least one count per energy bin in the range of 0.2-10 keV for XMM MOS, and 0.4-10 keV for XMM EPIC PN and *Suzaku*/XIS cameras, and modelled using C-statistics [33] in *Xspec* [34] for the initial fit where only priors on normalisation defined from the parallax were used. The parameter values and uncertainties were estimated using the the posterior samples generated with the `chain` command implementing a Markov chain Monte Carlo (mcmc) method in *Xspec*. On the other hand, for the final mass and radius estimates that include more complex priors (i.e. full distance priors and EOS priors from the literature) the Bayesian spectral analysis (*BXA*) package [35] was used to generate posterior samples.

Spectral analysis

Single temperature models

Several options were considered to model the observed X-ray spectrum. Taking into account that uniformly emitting hydrogen atmospheres or blackbody models were already shown to provide unrealistic neutron star parameters for distances around $\sim$ 3 kpc [14], we only considered an absorbed, uniformly emitting carbon atmosphere, and two kinds of models with non-uniform temperature distributions. For a uniformly emitting carbon atmosphere model, flat priors for mass, radius, and temperature were assumed, while Gaussian priors according to the observed zero-point corrected Gaia parallax were used to define the atmosphere model normalisation. In practice, this was done in the *Xspec* package where the normalisation of the *carbatm* component was tied to a hidden parameter equal to the zero-point corrected parallax value px as $norm = (10 \times px)^2 (px/px)$. Priors for the parallax were then set using the *bayes* command in *Xspec*. The fits were carried out and the uncertainties estimated from the *mcmc* chain created by running the *chain* command in *Xspec*.

In all cases (also those discussed in the next section), interstellar absorption was included in the model and described using a *TBabs* component with the abundances from [36]. Finally, for all models we also included a component associated with the dust scattering halo around the neutron star recently studied in detail by [20], and expected to contribute to the soft part of the spectrum. Indeed, scattered emission is softer than the incident flux, and a large fraction of the halo falls within the PSFs of XMM-*Newton* and *Suzaku*, respectively, making the observed spectrum somewhat softer. A similar component is commonly included in the modeling of the spectrum of the CCO in Cas A. To model this component, we used the *xscat* model in *Xspec* [37]. We assumed MRN [38] dust composition, with an effective hydrogen column density equal to that of the absorption component, and the relative distance to the observer fixed to the value reported by [20] based on the analysis of the radial halo profile using *Chandra* data for the thin sheet approximation, i.e. 0.88. We

note that while the actual dust distribution is likely more complex [20], this is not expected to significantly change the halo contribution to the point source spectrum. Inclusion of the scattering component was indeed found to only have a minor yet noticeable effect on the derived parameters as illustrated in Fig. M2. The best-fit parameters are reported in Table 1 and correspond to the thick solid contours in Fig. 1. The posterior samples are also available via http://samples.info.tobe.updated.after.clarificationonwhereelectronicdatagoes.

More complex temperature distributions

As already mentioned, emission from a NS surface with uniform temperature is not the only option to describe the observed X-ray spectrum. It may be that the temperature distribution over the surface is actually not uniform and pulsations are not observed only due to their low amplitude. To test the feasibility of this scenario, it is important to verify whether the observed spectrum agrees with the upper limits on pulsed fraction. The expected pulsed fraction is basically defined by the difference in temperatures of the polar and equatorial areas and orientation of the spinning neutron star with respect to the observer. To estimate the probability that the pulsations are missed because of an unfavorable orientation of the pulsar, one needs, therefore, to constrain the temperature distribution, which can be done based on the modeling of the observed X-ray spectrum. We therefore considered two kinds of spectral models to describe this situation: two-temperature models with hotter and cooler components intended to mimic emission from the polar areas and the rest of the surface (both described as either hydrogen or carbon atmospheres [39]), and a more realistic case with a smooth variation of temperature over the surface. In the latter case, hydrogen atmosphere models (similar to the uniformly distributed temperature case) yield completely unrealistic NS parameters, so only results for carbon atmospheres are reported.

For the two component models, strong degeneracy between component parameters required that most of the parameters remain fixed to some reasonable values. In particular, given that the main goal of the modeling here was to assess whether pulsations from a standard neutron star at a given distance could be missed, we assumed standard neutron star parameters and a fixed distance to the source, whereas the temperatures of the two components and fractional area occupied by the hotter component were considered as free parameters. On the other hand, the same parallax-based priors for normalization and flat priors for mass and radius as described in the previous section for the uniform temperature models were assumed for the more realistic models with smoothly varying temperature.

In the latter case, we used the same parametrisation of temperature over the surface as in [40]. Physically, this model is motivated by the assumption that the CCO has a strong buried magnetic field and a thermal flux through the neutron star crust driven by the inclination of the dipole field in the crust [41]. For a dipole magnetic field configuration, one might expect in this case a temperature distribution with zero temperature at the magnetic equator

Parameter	$carbatm_1$	$carbatm_2$	$hatm_2$	cd_0	cd_{90}
$N_{\rm H}, 10^{22}\,{\rm cm}^{-2}$	2.25(3)	2.22(2)	$2.69^{+0.04}_{-0.05}$	2.23(3)	2.26(2)
T_1, MK	$2.05^{+0.09}_{-0.06}$	≤ 1.04	1.07(2)	$2.09^{+0.06}_{-0.05}$	$2.28^{+0.07}_{-0.06}$
T_2, MK		$2.44^{+0.04}_{-0.03}$	3.97(4)		
f_1		0.977(2)	0.9976(1)		
$M/M_\odot$	$0.77^{+0.20}_{-0.17}$	1.4	1.4	0.89(18)	$0.78^{+0.32}_{-0.21}$
R, km	$10.4^{+0.86}_{-0.78}$	12	12	$11.69^{+1.02}_{-0.89}$	$11.84^{+2.34}_{-2.24}$
χ^2	2313.23	2312.98	2398.26	2313.64	2312.91
dof	2038	2039	2039	2038	2038

Table 1 Best fit results for spectral fits using only zero-point corrected parallax as a prior. Reported are values for a single temperature carbon atmosphere model ($carbatm_1$), two-temperature carbon and hydrogen atmosphere models ($carbatm_2$,$hatm_2$), and carbon atmosphere models with smooth temperature distribution and angle between the magnetic and spin axes of 0 and 90 degrees. The value of the parameter f_1 denotes the fraction of the surface of the neutron star occupied by the cooler component. Uncertainties are reported at 1σ confidence level.

given by $T^4 = T_p^4 4\cos\beta^2(1+3\cos\beta^2)^{-1}$, where T_p is the temperature at the pole, and β is the magnetic co-latitude [40]. Assuming the temperature distribution described above, and local spectra interpolated based on the existing *carbatm* grid, we computed a tree-parameter grid of the model spectra. The first parameter is the neutron star radius (from 8 to 15.5 km with steps of 0.5 km), the second parameter is the neutron star mass (from 0.5 to 2 solar masses with steps of 0.1 solar masses), and the third parameter is the polar temperature T_p (from 2 to 4 MK with steps of 0.25 MK). The observed spectra were then computed for two values of the angle between the rotation axis and the magnetic pole, $\theta_{\rm B}$=0 and 90 degrees. The methods of computation for the spectra were discussed in detail in [12]. The best-fit results are presented in Table 1. The fit results were then used to estimate the theoretically expected pulsed fraction, and were then compared with observed limits on the pulsed fraction as described in section 1.

Incorporating EOS priors in spectral modeling

A detailed discussion of all theoretically possible EOSs and the implications that our results might have for them is well beyond the scope of this work, so here we would like only to illustrate how the obtained results might affect constraints already obtained by other authors. Recently, [22] published a comprehensive analysis of nuclear-physics and multi-messenger astrophysics constraints on the EOS of cold dense matter, i.e. NICER observations of PSR J0740+6620 and PSR J0030+0451, tidal deformability constrains deduced from the gravitational wave events GW190425 and GW170817 (including their electromagnetic counterparts AT2017gfo and GRB170817A). This estimate was updated by [23] to include the latest mass and radius measurements for PSR J0740+6620 by [27]. In addition to those estimates we also include constraints by [24] based on the analysis of the burst spectra of the X-ray burster 4U 1702-429. In particular, we start with EOSs calculated by [22] and weights for those estimated based on the full set of constraints considered

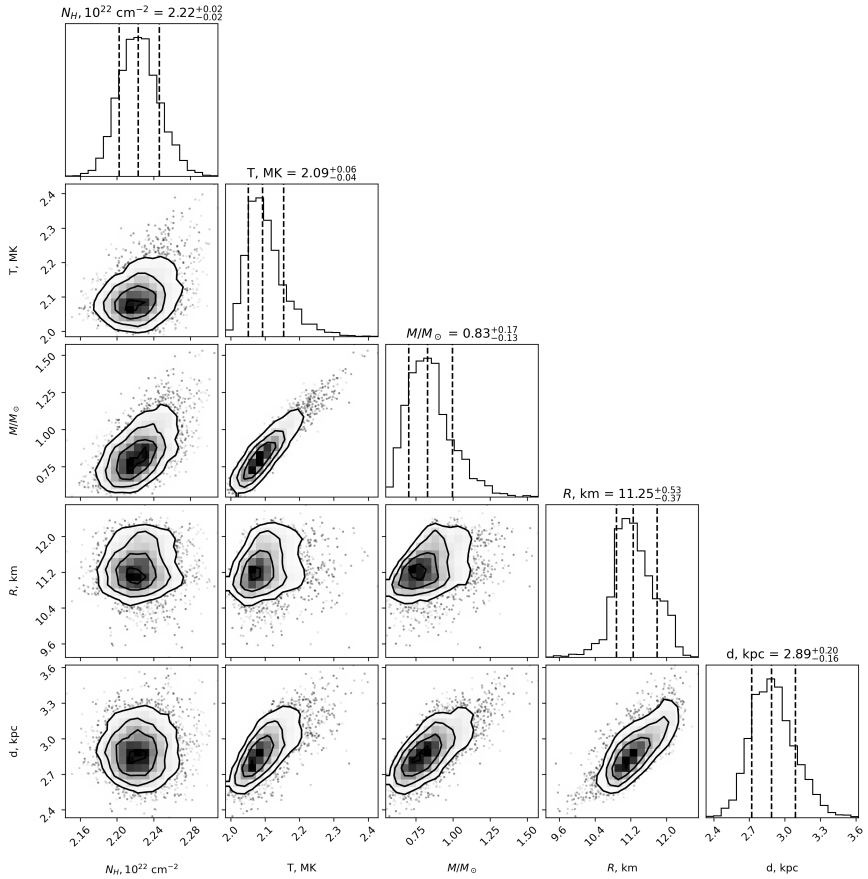

Fig. 2 Corner plots corresponding to the final fit with single temperature carbon atmosphere model including full distance priors and EOS constrain priors as discussed in the text.

by these authors (i.e. the `chiralEFT_MTOV_NICER_GW170817_AT2017gfo` family of solutions). We then adopt the same Bayesian procedure as these authors and [23] to incorporate mass and radius measurements from NICER (for PSR J0740+6620) and RXTE (for 4U 1702-429). That is, we assume that the likelihood of a given EOS is given by

$$\begin{aligned}\mathcal{L}_{\rm Burst}({\rm EOS}) &= \int dM dR\ p_{\rm Burst}(M,R)\pi(M,R\mid {\rm EOS}) \\ &\propto \int dM dR\ p_{\rm Burst}(M,R)\delta(R-R(M,{\rm EOS})) \\ &\propto \int dM\ p_{\rm Burst}(M,R=R(M,{\rm EOS})),\end{aligned} \tag{1}$$

where $p_{\rm Burst}(M,R)$ is the joint-posterior probability distribution from [24]. Here

we use the fact that the radius of the neutron star $R(M, EOS)$ is unambiguously defined for a given EOS. The likelihood is then marginalized over the entire parameter space. We verified that using this approach we were able to reproduce the results presented in [23] starting with those reported by [22] and including the most recent PSR J0740+6620 results, and then proceeded to also include constraints from 4U 1702-429 modeling to obtain the updated probabilities associated with each EOS.

These were then used to define priors for the modeling of the X-ray spectra taking all prior information into account. In practice this was accomplished using the Bayesian X-ray analysis (BXA) package [35]. In practical terms the EOS priors were incorporated within the BXA fit through interpolation over the two-dimensional look-up matrix in the mass/radius plane calculated based on posterior probabilities for individual EOSs obtained as described above. The matrix was calculated by co-adding posterior probabilities for all considered EOSs for each point on a grid (defined on a grid of 1000 steps for masses between 0.3 and 2 solar masses and for radii between 0.3 and 2.2), and used to derive NS radius priors for any given mass value (flat priors within the same range were assumed for the mass). In particular, priors for the radius were taken from the cumulative distribution of probability values within the look-up matrix row corresponding to the given mass value smoothed with a gaussian kernel with a width of $dM = 0.1 M_{\odot}$ (at each step of the fit, i.e. mass and radius priors are inter-dependent). Full Gaia distance priors were incorporated in the same way as in [20]. With priors defined, the BXA fit was carried out for the same set of spectra as in the simplified analysis described above, and the uncertainties for model parameters were estimated using the resulting posterior samples, i.e. we find $M = 0.83^{+0.17}_{-0.13} M_{\odot}$, $R = 11.25^{+0.53}_{-0.37}$ km as presented in Fig. 2. Note that all fit parameters are close to those reported above for the case when only parallax priors were considered, i.e. the quality of the fit for the X-ray spectra is comparable in both cases, although the formal assessment of the goodness of fit in the Bayesian framework is not straightforward in the absence of alternative models. The final posterior samples for all spectral fits along with the updated weights for all considered EOSs are available at http://updateafterclarificationoftheplaceforelectronicmaterial

To estimate the radius of the "standard" $1.4 M_{\odot}$ neutron star, and assess the impact of inclusion of our measurement in the context of tightening constraints on the EOS, we followed a procedure similar to that outlined above and used by [23]. In particular, the posterior samples obtained above were used to calculate the probability (or weight) of each of the considered EOS. The resulting weights were then used to select EOSs agreeing with the data at a specified confidence level (in our case 90% to permit a direct comparison with [23]), and the final $R_{1.4}$ value and confidence intervals were calculated by calculating the radius for $M = 1.4 M_{\odot}$ for the selected EOS. We have verified that we are able to reproduce the value reported by [23] when using only priors considered in that publication, and then proceeded with the inclusion of additional priors described above. With all extra priors included, we obtain $R_{1.4} = 11.68^{+0.52}_{-0.50}$ km, i.e. a

measurably narrower range compared to [23] who reports $R_{1.4} = 11.94^{+0.76}_{-0.87}$ km. We note that the inclusion of 4U 1702−429 data which was not considered by [23] also affects this estimate. A more direct comparison reflecting only the addition of the CCO results could be obtained by omitting the burster data, which leads to $R_{1.4} = 11.42^{+0.48}_{-0.43}$ km, i.e. slightly lower but with comparable uncertainties.

Timing analysis

Upper limits on pulsed fraction

Considering that one of the key assumptions in estimating neutron star parameters based on the spectral analysis is that the observed emission comes from the entire surface of the neutron star, it is important to justify this assumption, and the lack of detectable pulsations in CCOs is an important argument here. We attempted, therefore, to improve upper limits on the pulsed fraction by combining all available data from all telescopes with sufficient time resolution to search for pulsations in a given frequency range. We first extracted source photons from the same regions as for spectra (or columns corresponding to source position for timing modes) in the energy range of 1.7-4.2 keV, and corrected the observed photon arrival times to the Solar system barycentre. The energy range for the search was chosen to maximise the expected pulsed fraction based on the spectral modeling results and the observed background level. We then searched for possible pulsed signals using Z^2_2 statistics [42] as implemented in the *stingray* package [43]. To improve sensitivity, the periodicity search was conducted over period ranges listed in Table 2 and corresponding to the Nyquist frequencies for various XMM EPIC readout modes. The aim was to maximise counting statistics in each frequency range by including the maximum amount of data with a time resolution suitable for detecting pulsations (hence weaker limits for shorter periods which is due to the lower available exposure performed in high-resolution read-out modes).

Period range, s	Pulsed fraction limit, %	$P_{\rm H}$,%	$P_{\rm C}$,%	$P_{\rm dipole}$,%
$6 \times 10^{-5} - 3.5 \times 10^{-3}$	9.7	3.39	1.34	5.04
$3.5 \times 10^{-3} - 1.14 \times 10^{-2}$	5.2	1.23	0.48	1.80
$1.14 \times 10^{-2} - 0.1468$	3.8	0.75	0.29	1.08
0.1468-2000	3.4	0.62	0.24	0.90

Table 2 Upper limits on pulsed fraction and probability to miss pulsations by chance for a two-component carbon atmosphere model and a model with a smooth temperature variation as function of probed period range (at 3σ confidence level).

In each case, periodograms were averaged over segments with a length exceeding the longest period searched by a factor of 200 to reduce noise and further improve sensitivity. Similar to earlier works, no pulsed signal was found, so only upper limits on the pulsed fraction could be obtained (using the method outlined in [44] and implemented as *amplitude_upper_limit* and *pf_from_a stingray* functions in *Stingray*). As already mentioned, a non-detection

of the pulsations does not necessarily imply that the temperature distribution over the surface of the neutron star is fully uniform; however, the obtained upper limits together with the spectral analysis results can still be used to put strong constraints on the geometry of the potential pulsar and estimate the probability of missing pulsations by chance, which we discuss in the next section.

Theoretically expected pulsed fraction

The results of the spectral modeling described above were then used as input for calculation of the potentially expected pulsed fraction for arbitrary angles defining the geometry of the in-homogeneously emitting neutron star. In particular, we assume that potential pulsations arise because of higher temperature around the magnetic poles, and, therefore, the geometry is defined by two angles. That is, angle $\theta_{\rm B}$ between the magnetic dipole axis and the rotational axis, and inclination angle i between the rotational axis and the direction to the observer. The method for computing the pulsed fraction was described in detail for the two-temperature hydrogen model by [12], and takes into account gravitational light bending and local beam pattern expected based on atmosphere calculations. The same method has now been extended to two-temperature carbon atmosphere as well as carbon atmosphere models with a smoothly varying temperature profile described above. In both cases, we used fixed neutron star parameters, $M = 1.4 M_{\odot}$ and $R = 12\,$km, and the spot temperatures and their averaged visible area fractions presented in Table 1. The variability was investigated in the energy range 1.7-4.2 keV, where the amplitude of potential pulsations could be expected to be largest based on model atmosphere calculations and given the instrumental background level. The corresponding pulsed fraction maps for all three cases are shown in Fig. 3.

Compared to [12], the revised distance estimate further reduced the allowed hot spot area for the two-temperature hydrogen atmosphere model, and thus the range of angles compatible with the observed pulsed fraction limit. The obtained probability is now 6.2×10^{-3} (see Table 2). This value is uncomfortably low even for a single source. We also note that the joint probability to miss pulsations from all non-pulsating CCOs is even lower ($\sim 10^{-6}$ assuming blackbody-like hotspots [16]), so we conclude that it is highly unlikely that pulsations are not detected just because of an unfavourable orientation if emission from a two-temperature hydrogen atmosphere is assumed. Considering the larger derived hotspot area for a two-component carbon atmosphere, one could expect a higher chance of missing pulsations, which could thus provide an alternative explanation for their non-detection. We find, however, that the actual probability here is even lower than for the hydrogen atmosphere case (2.4×10^{-3}, see Table 2). This is due to the fact that emission from the carbon atmosphere is strongly beamed towards the normal (see e.g. Fig.3 in [12]), which is a direct consequence of the fact that the observed part of the spectrum is determined by the carbon photo-ionisation opacity. A specific intensity emitted at larger angles to the normal forms at cooler upper atmospheric layers where carbon is less ionised

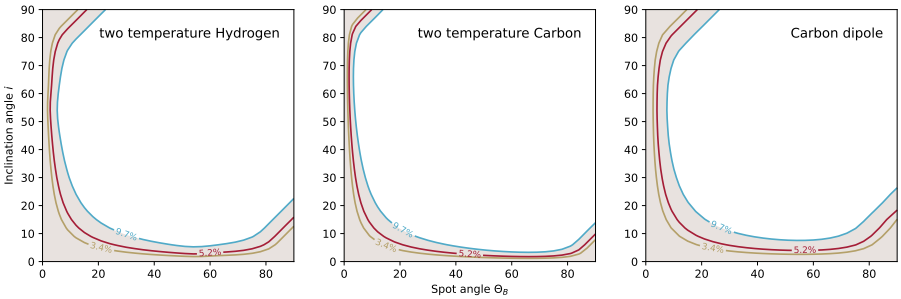

Fig. 3 The contours show the theoretically expected pulsed fraction given the best-fit spectral parameters for each model described in Section 1 and upper limits obtained in this work for various frequency ranges and reported in Table 2. The region to the lower-left of the respective contours represents the range of angles allowed for a given model and upper limit on pulsed fraction. The shaded region corresponds thus to the weakest of the upper limits (i.e. 9.7%) and represents a conservative estimate.

and photo-ionisation opacity is larger. We conclude, therefore, that the absence of observable pulsations due to unfavorable orientation is also unlikely in this scenario.

Finally, a similar approach was used for the neutron star model covered by a carbon atmosphere with a smoothed temperature distribution, as it was described in Sect. 1. We assumed the neutron star parameters, averaged between the two limiting cases $\theta_{\rm B} = 0$ and 90 degrees (see Table 1), namely $M = 0.83 M_{\odot}$, $R = 11.8$ km and $T_{\rm p} = 2.19$ MK as input since the difference in derived parameters is in any case small and can not meaningfully affect the results. The area of the hot neutron star part is larger in comparison with a local hot spot case, and as a consequence the estimated probability to miss pulsations because of unfavorable orientation is also slightly larger, (9×10^{-3}, see Table 2). However, it remains low even if only a single source is considered, so we conclude that the CCO is likely indeed not pulsating and we observe emission from a more or less uniformly hot carbon atmosphere.

Data and software availability

XMM-*Newton* and *Suzaku* data used in the publication are publicly available at the respective missions' data centres and HEASARC archives. The data reduction was carried out using the software and instructions provided by the respective mission science operation centres. The tabulated EOSs considered in this work are available as part of the original publications (i.e. [22–24]).

Acknowledgments. The scientific results reported in this article are based to a significant degree on observations made with the *Chandra* X-ray Observatory, and made use of software provided by the Chandra X-ray Center (CXC). This research also made use of observations obtained with XMM-*Newton*, an ESA science mission with instruments and contributions directly funded by ESA Member States and NASA. For analysing X-ray spectra, we use the analysis software BXA ([35]), which connects the nested sampling algorithm *UltraNest*

[45] with the fitting environment CIAO/Sherpa [46]. This research also made use of the *astropy* package [47]. The work was supported by the German Research Foundation (DFG) grant WE 1312/53-1 (VFS).

References

[1] Pavlov, G.G., Zavlin, V.E., Sanwal, D.: Thermal Radiation from Neutron Stars: Chandra Results. In: Becker, W., Lesch, H., Trümper, J. (eds.) Neutron Stars, Pulsars, and Supernova Remnants, p. 273 (2002)

[2] Pavlov, G.G., Sanwal, D., Teter, M.A.: Central Compact Objects in Supernova Remnants. In: Camilo, F., Gaensler, B.M. (eds.) Young Neutron Stars and Their Environments, vol. 218, p. 239 (2004)

[3] De Luca, A.: Central compact objects in supernova remnants. In: Journal of Physics Conference Series. Journal of Physics Conference Series, vol. 932, p. 012006 (2017). https://doi.org/10.1088/1742-6596/932/1/012006

[4] Halpern, J.P., Gotthelf, E.V.: Spin-Down Measurement of PSR J1852+0040 in Kesteven 79: Central Compact Objects as Anti-Magnetars. ApJ **709**(1), 436–446 (2010) arXiv:0911.0093 [astro-ph.HE]. https://doi.org/10.1088/0004-637X/709/1/436

[5] Gotthelf, E.V., Halpern, J.P., Alford, J.: The Spin-down of PSR J0821-4300 and PSR J1210-5226: Confirmation of Central Compact Objects as Anti-magnetars. ApJ **765**(1), 58 (2013) arXiv:1301.2717 [astro-ph.HE]. https://doi.org/10.1088/0004-637X/765/1/58

[6] Lattimer, J.M., Prakash, M.: The equation of state of hot, dense matter and neutron stars. **621**, 127–164 (2016) arXiv:1512.07820 [astro-ph.SR]. https://doi.org/10.1016/j.physrep.2015.12.005

[7] Degenaar, N., Suleimanov, V.F.: Testing the Equation of State with Electromagnetic Observations. In: Rezzolla, L., Pizzochero, P., Jones, D.I., Rea, N., Vidaña, I. (eds.) Astrophysics and Space Science Library. Astrophysics and Space Science Library, vol. 457, p. 185 (2018). https://doi.org/10.1007/978-3-319-97616-7_5

[8] Zavlin, V.E., Pavlov, G.G., Trumper, J.: The neutron star in the supernova remnant PKS 1209-52. Astr. Astrophys. **331**, 821–828 (1998) arXiv:astro-ph/9709267 [astro-ph]

[9] Pavlov, G.G., Luna, G.J.M.: A Dedicated Chandra ACIS Observation of the Central Compact Object in the Cassiopeia A Supernova Remnant. ApJ **703**(1), 910–921 (2009) arXiv:0905.3190 [astro-ph.HE]. https://doi.org/10.1088/0004-637X/703/1/910

[10] Klochkov, D., Pühlhofer, G., Suleimanov, V., Simon, S., Werner, K., Santangelo, A.: A non-pulsating neutron star in the supernova remnant HESS J1731-347/G353.6-0.7 with a carbon atmosphere. Astr. Astrophys. **556**, 41 (2013) arXiv:1307.1230 [astro-ph.HE]. https://doi.org/10.1051/0004-6361/201321740

[11] Elshamouty, K.G., Heinke, C.O., Morsink, S.M., Bogdanov, S., Stevens, A.L.: The Impact of Surface Temperature Inhomogeneities on Quiescent Neutron Star Radius Measurements. ApJ **826**(2), 162 (2016) arXiv:1605.09400 [astro-ph.HE]. https://doi.org/10.3847/0004-637X/826/2/162

[12] Suleimanov, V.F., Klochkov, D., Poutanen, J., Werner, K.: Probing the possibility of hotspots on the central neutron star in HESS J1731-347. Astr. Astrophys. **600**, 43 (2017) arXiv:1701.06417 [astro-ph.HE]. https://doi.org/10.1051/0004-6361/201630028

[13] Ho, W.C.G., Heinke, C.O.: A neutron star with a carbon atmosphere in the Cassiopeia A supernova remnant. Nature **462**(7269), 71–73 (2009) arXiv:0911.0672 [astro-ph.HE]. https://doi.org/10.1038/nature08525

[14] Klochkov, D., Suleimanov, V., Pühlhofer, G., Yakovlev, D.G., Santangelo, A., Werner, K.: The neutron star in HESS J1731-347: Central compact objects as laboratories to study the equation of state of superdense matter. Astr. Astrophys. **573**, 53 (2015) arXiv:1410.1055 [astro-ph.HE]. https://doi.org/10.1051/0004-6361/201424683

[15] Doroshenko, V., Suleimanov, V., Santangelo, A.: CXOU J160103.1-513353: another central compact object with a carbon atmosphere? Astr. Astrophys. **618**, 76 (2018) arXiv:1806.09946 [astro-ph.HE]. https://doi.org/10.1051/0004-6361/201833271

[16] Wu, Q., Pires, A.M., Schwope, A., Xiao, G.-C., Yan, S.-P., Ji, L.: What causes the absence of pulsations in Central Compact Objects in supernova remnants? Research in Astronomy and Astrophysics **21**(11), 294 (2021) arXiv:2109.06036 [astro-ph.HE]. https://doi.org/10.1088/1674-4527/21/11/294

[17] Halpern, J.P., Gotthelf, E.V.: Spin-Down Measurement of PSR J1852+0040 in Kesteven 79: Central Compact Objects as Anti-Magnetars. ApJ **709**(1), 436–446 (2010) arXiv:0911.0093 [astro-ph.HE]. https://doi.org/10.1088/0004-637X/709/1/436

[18] Doroshenko, V., Pühlhofer, G., Kavanagh, P., Santangelo, A., Suleimanov, V., Klochkov, D.: Evidence for a binary origin of a central compact object. MNRAS **458**(3), 2565–2572 (2016) arXiv:1508.03557 [astro-ph.HE]. https://doi.org/10.1093/mnras/stw499

[19] Bailer-Jones, C.A.L., Rybizki, J., Fouesneau, M., Demleitner, M., Andrae, R.: Estimating Distances from Parallaxes. V. Geometric and Photogeometric Distances to 1.47 Billion Stars in Gaia Early Data Release 3. AJ **161**(3), 147 (2021) arXiv:2012.05220 [astro-ph.SR]. https://doi.org/10.3847/1538-3881/abd806

[20] Landstorfer, A., Doroshenko, V., Pühlhofer, G.: Dust scattering halo around the CCO in HESS J1731-347: A detailed analysis. **659**, 82 (2022). https://doi.org/10.1051/0004-6361/202142334

[21] Lallement, R., Babusiaux, C., Vergely, J.L., Katz, D., Arenou, F., Valette, B., Hottier, C., Capitanio, L.: Gaia-2MASS 3D maps of Galactic interstellar dust within 3 kpc. Astr. Astrophys. **625**, 135 (2019) arXiv:1902.04116 [astro-ph.GA]. https://doi.org/10.1051/0004-6361/201834695

[22] Dietrich, T., Coughlin, M.W., Pang, P.T.H., Bulla, M., Heinzel, J., Issa, L., Tews, I., Antier, S.: Multimessenger constraints on the neutron-star equation of state and the Hubble constant. Science **370**(6523), 1450–1453 (2020) arXiv:2002.11355 [astro-ph.HE]. https://doi.org/10.1126/science.abb4317

[23] Pang, P.T.H., Tews, I., Coughlin, M.W., Bulla, M., Van Den Broeck, C., Dietrich, T.: Nuclear Physics Multimessenger Astrophysics Constraints on the Neutron Star Equation of State: Adding NICER's PSR J0740+6620 Measurement. ApJ **922**(1), 14 (2021) arXiv:2105.08688 [astro-ph.HE]. https://doi.org/10.3847/1538-4357/ac19ab

[24] Nättilä, J., Miller, M.C., Steiner, A.W., Kajava, J.J.E., Suleimanov, V.F., Poutanen, J.: Neutron star mass and radius measurements from atmospheric model fits to X-ray burst cooling tail spectra. Astr. Astrophys. **608**, 31 (2017) arXiv:1709.09120 [astro-ph.HE]. https://doi.org/10.1051/0004-6361/201731082

[25] Hessels, J.W.T., Ransom, S.M., Stairs, I.H., Freire, P.C.C., Kaspi, V.M., Camilo, F.: A Radio Pulsar Spinning at 716 Hz. Science **311**(5769), 1901–1904 (2006) arXiv:astro-ph/0601337 [astro-ph]. https://doi.org/10.1126/science.1123430

[26] Miller, M.C., Lamb, F.K., Dittmann, A.J., Bogdanov, S., Arzoumanian, Z., Gendreau, K.C., Guillot, S., Harding, A.K., Ho, W.C.G., Lattimer, J.M., et al.: PSR J0030+0451 Mass and Radius from NICER Data and Implications for the Properties of Neutron Star Matter. ApJ Letters **887**(1), 24 (2019) arXiv:1912.05705 [astro-ph.HE]. https://doi.org/10.3847/2041-8213/ab50c5

[27] Miller, M.C., Lamb, F.K., Dittmann, A.J., Bogdanov, S., Arzoumanian, Z., Gendreau, K.C., Guillot, S., Ho, W.C.G., Lattimer, J.M., Loewenstein, M.,

et al.: The Radius of PSR J0740+6620 from NICER and XMM-Newton Data. ApJ Letters **918**(2), 28 (2021) arXiv:2105.06979 [astro-ph.HE]. https://doi.org/10.3847/2041-8213/ac089b

[28] Suwa, Y., Yoshida, T., Shibata, M., Umeda, H., Takahashi, K.: On the minimum mass of neutron stars. MNRAS **481**(3), 3305–3312 (2018) arXiv:1808.02328 [astro-ph.HE]. https://doi.org/10.1093/mnras/sty2460

[29] Lindegren, L., Klioner, S.A., Hernández, J., Bombrun, A., Ramos-Lerate, M., Steidelmüller, H., Bastian, U., Biermann, M., de Torres, A., Gerlach, E., et al.: Gaia Early Data Release 3. The astrometric solution. Astr. Astrophys. **649**, 2 (2021) arXiv:2012.03380 [astro-ph.IM]. https://doi.org/10.1051/0004-6361/202039709

[30] Groenewegen, M.A.T.: The parallax zero-point offset from Gaia EDR3 data. Astr. Astrophys. **654**, 20 (2021) arXiv:2106.08128 [astro-ph.GA]. https://doi.org/10.1051/0004-6361/202140862

[31] Huang, Y., Yuan, H., Beers, T.C., Zhang, H.: The Parallax Zero-point of Gaia Early Data Release 3 from LAMOST Primary Red Clump Stars. ApJ Letters **910**(1), 5 (2021) arXiv:2101.09691 [astro-ph.GA]. https://doi.org/10.3847/2041-8213/abe69a

[32] Zinn, J.C.: Validation of the Gaia Early Data Release 3 Parallax Zero-point Model with Asteroseismology. AJ **161**(5), 214 (2021) arXiv:2101.07252 [astro-ph.GA]. https://doi.org/10.3847/1538-3881/abe936

[33] Cash, W.: Parameter estimation in astronomy through application of the likelihood ratio. ApJ **228**, 939–947 (1979). https://doi.org/10.1086/156922

[34] Arnaud, K.A.: XSPEC: The First Ten Years. In: Jacoby, G.H., Barnes, J. (eds.) Astronomical Data Analysis Software and Systems V. Astronomical Society of the Pacific Conference Series, vol. 101, p. 17 (1996)

[35] Buchner, J., Georgakakis, A., Nandra, K., Hsu, L., Rangel, C., Brightman, M., Merloni, A., Salvato, M., Donley, J., Kocevski, D.: X-ray spectral modelling of the AGN obscuring region in the CDFS: Bayesian model selection and catalogue. Astr. Astrophys. **564**, 125 (2014) arXiv:1402.0004 [astro-ph.HE]. https://doi.org/10.1051/0004-6361/201322971

[36] Wilms, J., Allen, A., McCray, R.: On the Absorption of X-Rays in the Interstellar Medium. ApJ **542**(2), 914–924 (2000) arXiv:astro-ph/0008425 [astro-ph]. https://doi.org/10.1086/317016

[37] Smith, R.K., Valencic, L.A., Corrales, L.: The Impact of Accurate Extinction Measurements for X-Ray Spectral Models. ApJ **818**(2), 143 (2016) arXiv:1602.07766 [astro-ph.HE]. https://doi.org/10.3847/0004-637X/818/

2/143

[38] Mathis, J.S., Rumpl, W., Nordsieck, K.H.: The size distribution of interstellar grains. ApJ **217**, 425–433 (1977). https://doi.org/10.1086/155591

[39] Suleimanov, V.F., Klochkov, D., Pavlov, G.G., Werner, K.: Carbon Neutron Star Atmospheres. ApJ Suppl. **210**(1), 13 (2014) arXiv:1311.6037 [astro-ph.HE]. https://doi.org/10.1088/0067-0049/210/1/13

[40] Schwope, A., Pires, A.M., Kurpas, J., Doroshenko, V., Suleimanov, V.F., Freyberg, M., Becker, W., Dennerl, K., Haberl, F., Lamer, G., et al.: Phase-resolved X-ray spectroscopy of PSR B0656+14 with SRG/eROSITA and XMM-Newton. arXiv e-prints, 2106–14533 (2021) arXiv:2106.14533 [astro-ph.HE]

[41] Greenstein, G., Hartke, G.J.: Pulselike character of uchlackbody radiation from neutron stars. ApJ **271**, 283–293 (1983). https://doi.org/10.1086/161195

[42] Buccheri, R., Bennett, K., Bignami, G.F., Bloemen, J.B.G.M., Boriakoff, V., Caraveo, P.A., Hermsen, W., Kanbach, G., Manchester, R.N., Masnou, J.L., et al.: Search for pulsed γ-ray emission from radio pulsars in the COS-B data. Astr. Astrophys. **128**, 245–251 (1983)

[43] Huppenkothen, D., Bachetti, M., Stevens, A.L., Migliari, S., Balm, P., Hammad, O., Khan, U.M., Mishra, H., Rashid, H., Sharma, S., Martinez Ribeiro, E., Valles Blanco, R.: Stingray: A Modern Python Library for Spectral Timing. apj **881**(1), 39 (2019) arXiv:1901.07681 [astro-ph.IM]. https://doi.org/10.3847/1538-4357/ab258d

[44] Vaughan, B.A., van der Klis, M., Wood, K.S., Norris, J.P., Hertz, P., Michelson, P.F., van Paradijs, J., Lewin, W.H.G., Mitsuda, K., Penninx, W.: Searches for Millisecond Pulsations in Low-Mass X-Ray Binaries. II. ApJ **435**, 362 (1994). https://doi.org/10.1086/174818

[45] Buchner, J.: UltraNest - a robust, general purpose Bayesian inference engine. The Journal of Open Source Software **6**(60), 3001 (2021) arXiv:2101.09604 [stat.CO]. https://doi.org/10.21105/joss.03001

[46] Freeman, P., Doe, S., Siemiginowska, A.: Sherpa: a mission-independent data analysis application. In: Starck, J.-L., Murtagh, F.D. (eds.) Astronomical Data Analysis. Society of Photo-Optical Instrumentation Engineers (SPIE) Conference Series, vol. 4477, pp. 76–87 (2001). https://doi.org/10.1117/12.447161

[47] Astropy Collaboration, Robitaille, T.P., Tollerud, E.J., Greenfield, P.,

Droettboom, M., Bray, E., Aldcroft, T., Davis, M., Ginsburg, A., Price-Whelan, A.M., et al.: Astropy: A community Python package for astronomy. Astr. Astrophys. **558**, 33 (2013) arXiv:1307.6212 [astro-ph.IM]. https://doi.org/10.1051/0004-6361/201322068